Published in final edited form as:
Mol Genet Metab. 2011 May ; 103(1): 51–59. doi:10.1016/j.ymgme.2011.02.002.

Blind sterile 2 (bs2), a hypomorphic mutation in *Agps*, results in cataracts and male sterility in mice

R. Liegel[a], **B. Chang**[b], **R. Dubielzig**[c], and **D.J. Sidjanin**[a,*]

[a] Department of Cell Biology, Neurobiology, and Anatomy, Medical College of Wisconsin, Milwaukee, WI 53226, USA

[b] The Jackson Laboratory, Bar Harbor, ME 04609, USA

[c] School of Veterinary Medicine, University of Wisconsin-Madison, Madison, WI 53706, USA

Abstract

Blind sterile 2 (*bs2*) is a spontaneous autosomal recessive mouse mutation exhibiting cataracts and male sterility. Detailed clinical and histological evaluation revealed that *bs2* mice have cataracts resulting from severely disrupted lens fiber cells. Analysis of *bs2* testes revealed the absence of mature sperm and the presence of large multinucleate cells within the lumens of seminiferous tubules. Linkage analysis mapped the *bs2* locus to mouse chromosome 2, approximately 45cM distal from the centromere. Fine mapping established a 3.1Mb *bs2* critical region containing 19 candidate genes. Sequence analysis of alkylglycerone-phosphate synthase (*Agps*), a gene within the *bs2* critical region, revealed a G to A substitution at the +5 position of intron 14. This mutation results in two abundantly expressed aberrantly spliced *Agps* transcripts: $Agps^{\Delta exon14}$ lacking exon 14 or $Agps^{exon\Delta 13-14}$ lacking both exons 13 and 14 as well as full-length *Agps* transcript. Agps is a peroxisomal enzyme which catalyzes the formation of the ether bond during the synthesis of ether lipids. Both aberrantly spliced $Agps^{\Delta exon14}$ and $Agps^{exon\Delta 13-14}$ transcripts led to frame shift, premature stop and putative proteins lacking the enzymatic FAD domain. We present evidence that *bs2* mice have significantly decreased levels of ether lipids. Human mutations in *Agps* result in rhizomelic chondrodysplasia punctata type 3 (RCDP3), a disease for which *bs2* is the only genetic model. Thus, *bs2* is a hypomorphic mutation in *Agps*, and represents a useful model for investigation of the tissue specificity of ether lipid requirements which will be particularly valuable for elucidating the mechanism of disease phenotypes resulting from ether lipid depletion.

Keywords

Agps; ether lipids; peroxisome; RCDP3; cataract; mouse model

INTRODUCTION

Peroxisomes are ER-derived organelles present in most mammalian cells [1–6]. They are simple in structure and are comprised of a single membrane and about 50 proteins. All

*Corresponding author: D.J. Sidjanin, Department of Cell Biology, Neurobiology, and Anatomy, Human and Molecular Genetics Center, Medical College of Wisconsin, Milwaukee, WI 53226, dsidjani@mcw.edu, Phone: 414-456-7810, Fax: 414-456-6516.

Conflict of Interest Statement:
The authors declare no conflict of interest.

peroxisomal proteins are encoded by nuclear genes, synthesized on free ribosomes and are postranslationally imported. The molecular mechanisms of peroxisomal protein import have been recently reviewed [7], indicating a complex mechanism capable of transporting folded and oligomeric proteins across the membrane [8,9]. The vast majority of peroxisomal proteins contain peroxisome targeting signal 1 (PTS1)[6], a C-terminal Ser-Lys-Leu consensus sequence [10] that binds to the PTS1 receptor which mediates import into the peroxisome [11]. However, a small subset of peroxisomal proteins are imported via an alternative mechanism involving the N-terminal Arg/Lys-Leu-X5-Gln/His-Leu peroxisomal targeting signal 2 (PTS2) [6] and corresponding PTS2 receptor [12–15]. Peroxisomal proteins play a role in peroxisomal biogenesis and at least eight independent metabolic pathways including α- and β-oxidation of fatty acids, catalytic decomposition of hydrogen peroxide, and ether lipid synthesis [2,6,16]. The essential roles of peroxisomal function in mammals are reflected by a number of hereditary peroxisomal disorders in humans. Clinical phenotypes in these disorders may result from mutations in genes essential for peroxisomal formation, fusion, protein import, or functional defects of individual peroxisomal proteins.

Peroxisomal disorders are typically classified into two groups: peroxisomal biogenesis disorders (PBD), and isolated peroxisomal enzyme deficiencies [17–19]. The PBD group includes Zellweger spectrum disorders in which affected patients exhibit variable clinical phenotypes, most commonly including craniofacial dysmorphism, profound neurological abnormalities, severe psychomotor retardation, hypotonia, neonatal seizures, glaucoma, retinal degeneration and impaired hearing [17–19]. Mutations in at least 11 peroxisomal genes (*PEX1,2,3,5,6,10,12,13,14,16,19,* and *26)* have been identified as being associated with the Zellweger spectrum disorders[19,20]. These genes play an essential role in peroxisome biogenesis, and/or peroxisomal PTS1 protein import [17–19]. In addition to Zellweger spectrum disorders, rhizomelic chondrodysplasia punctata type 1 (RCDP1) is also classified within the PBD group of disorders. Mutations in *PEX7*, the gene encoding the PTS2 receptor, cause RCDP1 [12–14]. Clinical phenotypes of RCDP1 patients differ greatly from patients affected with Zellweger spectrum disorders. RCDP1 patients exhibit severe shortening of rhizomelic bones, bilateral cataracts, severe growth and motor delays, dysmorphic facial characteristics, stippled epiphyses, and vertebral coronal cleft [17,21,22]. Unlike RCDP1, rhizomelic chondrodysplasia punctata type 2 (RCDP2) and rhizomelic chondrodysplasia punctata type 3 (RCDP3) are classified as isolated peroxisomal enzyme deficiency disorders, resulting from mutations in glyceronephosphate O-acyltransferase (*GNPAT*) and alkylglycerone phosphate synthase (*AGPS)* respectively [23,24]. Interestingly, while only a single enzyme is deficient, RCDP2 and RCDP3 patients exhibit clinical phenotypes identical to those observed in RCDP1 patients. AGPS and GNPAT are peroxisomal enzymes required for the synthesis of plasmalogens, a class of ether lipid species containing a vinyl ether bond at the *sn-1* position of the glycerol backbone [24]. AGPS is one of the few peroxisomal proteins that is imported via the PTS2 signal/PEX7 receptor mechanism [2]. Although in RDCP1 all PTS2-mediated protein import is compromised, it has been shown that the RCDP1 phenotype is primarily determined by a loss of AGPS function [25]. Thus, disruption of the plasmalogen synthesis pathways has been established as the primary defect associated with clinical outcomes for all three forms of RCDP.

To better understand the molecular etiology of RCDP disorders, as well as the role of plasmalogens *in-vivo*, mouse models carrying null alleles of *Pex7* and *Gnpat* were previously generated as models for *RCDP1* and *RCDP2* [26,27]. Both *Pex7*$^{-/-}$ and *Gnpat*$^{-/-}$ mice exhibit cataracts and male sterility phenotypes [26,27]. To our knowledge, *Agps* null mice have not yet been described. In this study we show that *blind sterile 2* (*bs2*), a spontaneous mouse mutation identified to exhibit cataracts and male sterility [28], is a hypomorphic mutation in *Agps* resulting in severe plasmalogen deficiency. We also show

that *bs2* is not allelic with another spontaneous mouse mutation called blind sterile (*bs*) which like *bs2* exhibits phenotypes of cataracts and male sterility and maps to chromosome 2 [29,30]. As such, *bs2* represents the first genetic model of RCDP3, further providing an opportunity for evaluation of the role of *Agps in-vivo*. In addition, the availability of the *bs2* mouse mutant allows for comparative analysis between mouse and human phenotypes associated with all forms of *RCDP*.

MATERIALS AND METHODS

Mice, clinical evaluation, and histology

CAST/EiJ, C57BL/6, *bs* and *bs2* mice were all obtained from The Jackson Laboratory (Bar Harbor, ME). All mice showed normal life expectancy and breeding patterns with the exception of *bs* and *bs2* homozygote males which, consistent with previous results, were unable to produce litters [28,30]. Mouse eyes were examined with a Topcon SL-D8Z slit lamp biomicroscope with a Nikon SLR-based Photo Slit Lamp imaging system following mydriasis with 1% Atropine Sulfate (Bausch & Lomb). For WT and *bs2* histology, tissues were fixed in Zinc-formalin, or Davidson's solution, embedded in paraffin and sectioned to 4 microns thickness as previously described [31]. Following H&E staining, sections were mounted and photographed with a Nikon DS-Fi1 camera on a Nikon Eclipse 80i microscope.

Linkage Analysis

The *bs2* locus has been maintained on the congenic C57BL/6 background. For linkage studies, given that *bs2/bs2* male mice are sterile, *bs2/bs2* female mice were outcrossed to CAST/EiJ; the resulting F1 progeny were subsequently intercrossed to generate 262 F2 progeny. At four weeks of age F2 progeny were clinically evaluated for the presence of cataract as described above. F2 progeny were euthanized and tissues were collected. Genomic DNA was purified from collected tissues and initially genotyped with *D2Mit1, D2Mit465, D2Mit64, D2Mit7, D2Mit205, D2Mit247, D2Mit389, D2Mit459, D2Mit408, D2Mit260, D2Mit51, D2Mit457* as previously described [32]. Subsequent fine mapping analysis was performed on F2 progeny utilizing *D2Mit327, D2Mit245, D2Mit37, D2Mit219, D2Mit435, D2Mit93*, and *D2Mit183* as previously described [32]. Microsatellite alleles were scored following electrophoresis on a 2.5% agarose gel and EtBr staining. Linkage data was analyzed with MapManager QTX (http://www.mapmanager.org/mmQTX.html).

Genomic and cDNA sequence analysis

For sequence evaluation of exons and intron/exon junctions, primers (Table 1) were designed to anneal in introns about 50 bp from intron/exon junctions as previously described [32]. For cDNA analysis RNA was isolated from mouse tissues or tissue cultures, reverse transcribed, and PCR amplified using primers in Table 1. All generated PCR products were electrophoresed, gel-purified and sequenced as previously described [31]. Comparative sequence analysis was performed using DNAStar software (Madison, WI). For semi-quantitative analysis of *Agps* transcript levels, RT-PCR products were generated while in the exponential phase of PCR amplification using *Gapdh* as an internal control (Table 1). PCR band intensities were quantified using ImageJ software (http://rsbweb.nih.gov/ij/) and are expressed relative to *Gapdh.* The results represent at least three independent experiments performed in triplicates. Comparison between WT and *bs2* groups was analyzed by the Student's *t*-test and the data is expressed as mean ± SEM. A value of $p<0.05$ was designated as being statistically significant. The IVS 14+5G>A substitution in *Agps* identified as being responsible for the *bs2* phenotype introduces an *AluI* restriction site which allowed us to develop a genotyping assay. Primers were designed to amplify a 496 bp *Agps* genomic fragment that spans exon 14 and a portion of intron 14. The generated PCR products were

digested with *AluI* (NEB) following the manufacturer's protocol, separated on a 1.5% agarose gel, and scored. Following *AluI* digestion, the 496 bp PCR product containing the WT *Agps* IVS14+5G allele results in 3 fragments: 394 bp, 68 bp and 34 bp; the PCR product containing the *bs2 Agps* IVS14+5A results in 4 fragments: 248 bp, 146 bp, 68 bp and 34 bp.

Mass spectrometry

Mouse brains from age-matched pairs (ranging from 4–10 weeks) of *bs2* and WT siblings were collected and homogenized in a Dounce homogenizer in 1.0 ml of PBS. Lipids were extracted with 1:1:0.5 chloroform: methanol: water. The combined organic phases were washed once with 0.5 ml of KCl (1 M) followed by 0.5 ml of water, dried at 40°C under N_2 gas, and stored at −80°C. For phospholipid profiling, an electrospray ionization-tandem mass spectrometry approach was used, as previously described [33].

Cell culture, western blot, and immunocytochemistry analysis

Mouse embryonic fibroblasts (mEFs) were isolated from E13.5 mouse embryos and maintained as previously described [31]. For western blot analysis, mEFs were lysed with 0.5 ml RIPA buffer (Sigma) containing protease inhibitor cocktail (Sigma). Cell lysates were boiled for 5 min in Laemmli buffer containing β-ME, and separated on a 10% SDS-PAGE gel (all from Bio-Rad). Proteins were transferred at 100V to a PVDF membrane and blocked in 10% milk in 1xPBST for 1 hour. The blots were incubated overnight in 1x PBST containing either 1:2500 rabbit polyclonal catalase (Abcam) or 1:500 rabbit polyclonal Pmp70 (Abcam) primary antibodies. 1:5000 HRP-conjugated β-actin primary antibody (Abcam) was added to each primary incubation as a loading control. After three 10 minute washes in 1x PBST, 1:5000 Peroxidase-conjugated AffiniPure Donkey Anti-Rabbit IgG (H +L) (Jackson ImmunoResearch) was incubated in 1x PBST with the blot for 1 hour at 4°C. The detection was performed using the ECL Western Blot Analysis System (Amersham) following the manufacturer's instructions. In immunocytochemical studies, mEFs were grown on coverslips until reaching 50–70% confluency. The cells were fixed for 10 min in 4% PFA, washed 3x for 5 min with 1x PBS, and incubated overnight at 4°C in 1x PBST containing 1:1000 rabbit polyclonal catalase or 1:250 rabbit polyclonal PMP70 primary antibody (both Abcam). Cells were again washed 3x for 5 min with 1xPBS and incubated with 1:1000 Alexa 488-conjugated Goat-anti-rabbit secondary (Invitrogen) for 1hr at room temperature. Slides were mounted using Vectashield w/DAPI (Vector Labs), and imaged using a Nikon DS-Fi1 camera on a Nikon Eclipse 80i microscope.

Complementation studies

To determine if *bs* and *bs2* are allelic loci, *bs/bs* females were outcrossed to *bs2/+* males. 34 progeny from 6 litters were generated. Progeny were clinically evaluated for cataracts between 6 and 8 weeks of age as described above. For genotyping, 1 mm tail clippings were collected and boiled in 300 μl of 50 mM NaOH for 15 min, neutralized with 26 μl of 1M Tris pH8.0, and spun at 12,000g for 6 min. 2ul of the supernatant was used for PCR genotyping of the *bs2* allele as described above.

RESULTS

bs2 phenotypes

Analysis with slit-lamp biomicroscopy, following mydriasis, confirmed the previously reported *bs2* cataract phenotype (Figure 1B) [28]. Histological analysis of *bs2* eyes identified smaller globes and severely disrupted lenses (Figure 1D). Although lens epithelial cells at the anterior of the lens appeared normal, fiber cells within the bow region of the lens were smaller in size and were detached from the epithelium (Figure 1F). Bladder cells and

liquefied lens material were present within the cortex; morgagnian globules were noted at the posterior poles (Figure 1F). Except for the lens, no ocular structural defects were observed in *bs2* histological sections. Consistent with the initial report [28], breeding of *bs2* homozygote males did not produce any litters. Evaluation of *bs2* testes revealed that the testes are smaller in size when compared to WT controls (Figure 2A). Histological analysis in *bs2* sections identified severely disrupted seminiferous tubules (Figure 2D) and the absence of mature spermatozoa and elongating spermatids (Figure 2E). In addition, multinucleate cells were present within the lumen of the *bs2* seminiferous tubules (Figure 2E).

Positional cloning of the *bs2* locus

The initial report established linkage of the *bs2* locus to mouse chromosome 2, but did not implicate a specific chromosomal location [28]. To further map the *bs2* locus, we utilized an intercross breeding strategy to generate 262 F2 progeny. At four weeks of age 15% (39/262) of F2 progeny were identified as affected, thus deviating from the expected 25% Mendelian ratio for a recessive locus as evaluated by chi square ($p<0.05$). F2 progeny were genotyped with Chr. 2 microsatellites spaced approximately 10 cM apart. The results confirmed linkage of *bs2* to chromosome 2. The *bs2* locus was assigned as closest to *D2Mit247* in a region between *D2Mit205* and *D2Mit239* (Figure 3A). To further refine the genetic position of *bs2*, we genotyped the F2 progeny with microsatellites between *D2Mit205* and *D2Mit239.* This analysis established the *bs2* critical region as between *D2Mit219* and *D2Mit159*, encompassing a 3.1 Mb physical region (Figure 3B). Analysis of the mouse genome sequence (July 2007 build) revealed that the *bs2* critical region encompasses 19 previously established genes and one hypothetical gene (Table 2). In order to prioritize sequencing, we evaluated the NCBI (http://www.ncbi.nlm.nih.gov/gene/) and MGI databases (http://www.informatics.jax.org/) to identify if known mutations in any genes within the *bs2* critical region were reported to lead to cataracts or male sterility in humans or mice. This analysis led to identification of cytochrome c, testis (*Cyct;* **NM_009989**) a gene exclusively expressed in the testes; $Cyct^{-/-}$ null mice exhibit reduced sperm counts, impaired fertilization, and testicular atrophy [34]. The second candidate gene selected was alkylglycerone phosphate synthase (*Agps;* **NM_172666**) a ubiquitously expressed peroxisomal protein present in all mammalian cells; mutations in *AGPS* result in RCDP3 where affected patients exhibit congenital cataracts as a part of their syndromic phenotype [35]. Thus, we proceeded to evaluate both *Cyct* and *Agps* for mutations in *bs2* mice. Sequence analysis of *Cyct* exons, intron/exon junctions, and cDNA did not identify any sequence differences between WT and *bs2* mice (data not shown). Sequence analysis of *Agps* cDNA from WT mEFs identified a single *Agps* transcript that matched the full-length *Agps* sequence (NM_172666.2). In contrast, three *Agps* transcripts were identified in *bs2* mEFs (Figure 4A): full-length *Agps* transcript, $Agps^{\Delta exon14}$ which lacks exon 14, and $Agps^{exon\Delta 13–14}$ which lacks both exons 13 and 14 (Figures 4B and 4C). Full-length *Agps* transcript in *bs2* mEFs comprised only 7% of total *Agps* transcript (Figure 4C). Both $Agps^{exon\Delta 14}$ and $Agps^{exon\Delta 13–14}$ are predicted to result in a frameshift followed by a premature stop codon and truncated $Agps^{Glu467fsX474}$ and $Agps^{Phe441fsX456}$ proteins, respectively (Figure 4E). The same aberrantly spliced transcripts as well as relative abundances of full-length *Agps* were also observed in *bs2* lens, testes, spleen, and liver whereas only the single full-length transcript was observed in the same tissues of WT controls (not shown).

To further investigate the molecular basis for the aberrant *Agps* splicing observed in *bs2*, we sequenced the 12.3kb genomic region between exon 12 and exon 15. In *bs2*, sequence analysis identified a G to A substitution in *Agps* IVS14+5 (Figure 5A). The G nucleotide in *Agps* IVS14+5 is a part of the consensus 5′ splice sequence (Figure 5B). All affected

intercross animals genotyped A/A at *Agps* IVS14+5, while none of the unaffected mice genotyped A/A, indicating co-segregation of Agps IVS14+5A with the *bs2* phenotype. Evaluation of the SNP database did not reveal any previously reported polymorphisms for *Agps* intron 14 (http://www.ncbi.nlm.nih.gov/SNP/snp_ref.cgi?locusId=228061). Furthermore, we evaluated the *Agps* IVS14+5 locus in C57BL6/J, CAST/EiJ, AKR/J, C3H, RIIIS/J, DBA1/J, and DBA2/J strains and identified only G/G genotypes (not shown). These findings collectively suggest that the identified *Agps* IVS14+5G->A substitution is most likely responsible for the aberrant *Agps* splicing observed in *bs2*.

Mass spectrometry of lipid species

Both $Agps^{exon\Delta 14}$ and $Agps^{exon\Delta 13–14}$ are predicted to result in truncated non-functional proteins. In *bs2* mice, the remaining full-length *Agps* transcript represents only 15% of *Agps* levels observed in WT mice (Figure 4D). Thus, the *bs2* mutation most likely results in severely reduced functional Agps protein levels that would in turn result in a severe reduction of plasmalogens. To test this hypothesis, we analyzed brain phospholipid levels by mass spectrometry in WT and *bs2* mice. The *bs2* brains contained only 15% of the levels of ether-phosphatidyl ethanolamine (ePE) detected in brains from WT mice (Figure 6B). Similarly, in *bs2* samples, ether-phosphatidyl choline (ePC) levels were 35.1% of the levels of ePC observed in WT brains (Figure 6D). Interestingly, accumulation of phosphatidylethanolamine (PE), the precursor to ePE (Figure 6A), was detected in *bs2* brains; no accumulation of phosphatidylcholine (PC), precursor to ePC, was observed (Figure 6C).

Peroxisomal assembly and PTS-mediated protein import

To determine if peroxisomal assembly and PTS1 or PTS2 mediated peroxisomal protein import were compromised in *bs2*, we evaluated *bs2* mEFs. Immunofluorescence of WT and *bs2* mEFs with Pmp70, catalase (not shown), and peroxisomal thiolase (not shown) antibodies revealed a typical peroxisomal punctate staining pattern (Figure 6B). Western blotting did not show any difference in protein levels of Pmp70 (Figure 7C), catalase (Figure 7D), and thiolase (not shown) between WT and *bs2* mEFs. These findings suggest that peroxisome assembly as well as PTS1 and PTS2 mediated peroxisomal protein import did not differ between WT and *bs2* mEFs.

Examining possible allelism between *bs2* and *bs*

The lens and testicular phenotypes in *bs2* mice reported in this study resemble the phenotypes reported for the *blind sterile* (*bs*) mouse, another spontaneous mouse mutation on chromosome 2 resulting in cataracts and male sterility [29,30]. The genetic position for *bs* was previously assigned to chromosome 2 between *Hao1* and *Emv-15* loci suggesting that *bs* and *bs2* most likely are mutations in two separate genes on chromosome 2 resulting in similar cataract and male infertility phenotypes [29,30]. To exclude the possibility that *bs* and *bs2* are allelic, we set up a cross between *bs/bs* females and *bs2/+* males, generating 34 F1 progeny. Genotyping revealed that 12 F1 progeny carried the *Agps* IVS14+5A allele, indicating 12/34 were compound *bs* and *bs2* heterozygote mice. Clinical evaluation of all F1 progeny at >6 weeks of age did not identify any cataracts. Fertility in male *bs/bs2* compound heterozygotes did not differ from WT mice.

Discussion

In this study, our goal was to identify a gene and mutation responsible for the *bs2* cataract and male sterility phenotypes. Utilizing a positional cloning approach, we identified an IVS14+5G→A substitution in the 5′ splice site of *Agps* intron 14 as the causative mutation. The +5G position of the 5′ splice site is part of a consensus splice-donor sequence conserved

across species which base pairs with U1 snRNA to initiate splicing [36,37]. Positions −1 and +5 of the 5′ splice site base pair strongly with U1 snRNA, thus mutations at these positions have detrimental effects on splicing [37]. It has been recently established that 19.7% of diseases resulting from mutations in the 5′ splice sites are due to a mutation of the +5 nucleotide [36,38,39]. In *bs2* mice the *Agps* IVS14+5G→A substitution resulted in skipping of exon 14 or both exons 13 and 14 and the formation of the aberrantly spliced $Agps^{\Delta exon14}$ and $Agps^{exon\Delta13–14}$ transcripts. In addition to the two aberrantly spliced transcripts, we also identified a full length *Agps* transcript expressed at very low levels in *bs2* compared to WT mice. The putative mutant Agps proteins, $Agps^{Glu467fsX474}$ and $Agps^{Phe441fsX456}$, would have frameshifts following Thr467 and Phe441, respectively, resulting in a premature stop codon. Both putative proteins would be truncated near the start of the C-terminal catalytic FAD oxidase domain and thus, would be catalytically inactive. Agps is a member of the FAD binding oxidoreductase/transferase type 4 family of proteins. The role of Agps is to catalyze the second step of ether lipid biosynthesis in which acyl-dihydroxyacetonephosphate (DHAP) is converted to alkyl-DHAP [24]. Phospholipid profiling of *bs2* brains identified severely reduced ether-lipid levels further confirming that the *bs2* phenotypes are associated with a disruption in the ether-lipid synthesis pathway. Ether-lipids were observed in *bs2* brains at low levels, most likely resulting from the Agps activity encoded by the small fraction of properly spliced *Agps* transcript identified in *bs2* tissues. These findings collectively show that *bs2* is a hypomorphic mutation in *Agps* resulting in disruption of the ether lipid synthesis pathway, leading to a severe reduction of ether lipid levels.

Mutations in *AGPS* have been previously reported in only three RCDP3 patients [23,35,40]. Biochemical evaluation of fibroblasts from RCDP3 patients identified deficient AGPS enzymatic function and severely reduced plasmalogen levels [40,41]. RCDP3 fibroblasts, similarly to RCDP2 fibroblasts, exhibit ether lipid deficiencies due to mutations in enzymes essential for ether lipid synthesis without defects in peroxisomal assembly and PTS1 or PTS2 mediated protein import [40,42]. A mutation in *AGPS* was also identified in a plasmalogen-deficient CHO cell line following a mutagenesis screen [43]. Analysis of the plasmalogen deficient CHO line identified significantly reduced AGPS enzymatic function with intact peroxisomal assembly and protein import [43]. Functional evaluation of *bs2* mEFs is consistent with these findings, indicating that *Agps* IVS14+5G→A results in a severe reduction of Agps function. In addition, we did not observe any difference in PTS1 and PTS2 mediated protein import or peroxisomal assembly between WT and *bs2*. Therefore, the severe loss of ether lipids observed in *bs2* mice is the result of a mutation in *Agps* in which the resulting enzymatic deficiency is independent of peroxisomal assembly or peroxisomal protein import. As such, the *bs2* mouse is the first animal model of RCDP3, providing an excellent opportunity for evaluation of Agps deficiency *in-vivo*.

The mechanism by which an overall reduction of plasmalogen levels results in tissue-specific RCDP phenotypes in humans and mice is not well understood. Plasmalogens contribute to about 18% of total phospholipid mass, although there is a unique tissue-specific distribution: ePE levels are high in brain, heart, lung, kidney, spleen, and testis whereas high levels of ePC were noted in the cardiac and skeletal muscles [2,24]. Originally, the *bs2* mouse was identified during a phenotypic screen of mice with spontaneous mutations exhibiting vision defects [28]. The initial study reported cataracts in *bs2* mice [28]. Results from this study show that *bs2* cataracts are associated with defects in the elongation of lens fiber cells. Histological evaluation further showed that attenuated lens fiber cells were also detached from the lens epithelium, suggesting either a defect in lens fiber elongation or defect in cell-to-cell communication between lens epithelial and fiber cells. The cataract phenotype was also reported for $Pex7^{-/-}$ and $Gnpat^{-/-}$ mice [26,27]. Similarly, all patients affected with RCDP are either born with cataracts or develop cataracts

within the first six months of life [21,25]. These findings suggest that plasmalogens are essential for lens development and homeostasis in both humans and mice. Recently, analysis of mouse lenses identified ePE as the major ether lipid class in the lens although ePC, phosphatidyl serine, and sphingomyelin were also present [44]. It has been proposed that plasmalogens may be protecting lens membranes against oxidative stress and may be essential for signaling [44]. Further evaluation is necessary for better understanding of the role of plasmalogens in the lens.

In addition to cataracts, all three RCDP mouse models, *Pex7*$^{-/-}$, *Gnpat*$^{-/-}$, and *bs2*, exhibit disorganized seminiferous tubules with abnormalities in spermatogenesis resulting in testicular atrophy and male sterility [26,27]. Loss of plasmalogens in the testes of *Gnpat*$^{-/-}$ mice was associated with down-regulation and mis-targeting of claudin-3 and consequent impairment of the blood-testis-barrier leading to deficient sealing of the transient intermediate compartment [45]. In addition to cataracts and testicular phenotypes, *bs2* mice exhibited some prenatal/perinatal lethality which was also observed in *Pex7*$^{-/-}$ and *Gnpat*$^{-/-}$ mice [26,27]. The cause of prenatal/perinatal lethality associated with a decrease in ether lipids remains unclear. Interestingly, in *bs2* we did not observe any obvious hypotonia, delayed growth, defects in neuronal migration, or bone ossification defects reported for *Pex7*$^{-/-}$ [26] or myelination defects reported for *Gnpat*$^{-/-}$ [27,46]. These differences may be due to residual plasmalogen levels present in *bs2* tissues, suggesting that the severity of the phenotype in mice may be associated with plasmalogen levels. This is consistent with findings in patients affected with all forms of RCDP in which disease severity is directly related to plasmalogen levels [25,47].

Finally, as a part of this study we showed that *bs2* is not allelic with *bs*, a mouse model also exhibiting cataracts and male sterility that was previously mapped to chromosome 2 [29,30]. This finding confirms that *bs2* is the only genetic model for RCDP3. Further analysis of pathways implicated in the *bs* phenotype may yield additional information on the mechanism of the tissue specificity observed in both blind-sterile mouse models. In combination with existing RCDP models, the *bs2* mouse provides an exciting opportunity to facilitate a better understanding of the molecular consequences and mechanisms involved in ether-lipid deficiency.

Supplementary Material

Refer to Web version on PubMed Central for supplementary material.

Acknowledgments

This work was supported in part by National Institutes of Health grants EY15173 (D.J.S), and EY19943 (B.C). The lipid analyses described in this work were performed at the Kansas Lipidomics Research Center Analytical Laboratory. Kansas Lipidomics Research Center was supported by National Science Foundation (EPS 0236913, MCB 0455318, DBI 0521587), Kansas Technology Enterprise Corporation, K-IDeA Networks of Biomedical Research Excellence (INBRE) of National Institute of Health (P20RR16475), and Kansas State University.

ABBREVIATIONS

bs2	blind-sterile 2
Agps	alkylglyceronephosphate synthase
RCDP3	Rhizomelic chondrodysplasia punctata type 3
PTS1	peroxisomal targeting signal 1
PTS2	peroxisomal targeting signal 2

FAD	flavin adenine dinucleotide
PBD	peroxisomal biogenesis disorders
RCDP1	rhizomelic chondrodysplasia punctata type 1
RCDP2	rhizomelic chondrodysplasia punctata type 2
GNPAT	glyceronephosphate O-acyltransferase
PEX7	peroxisomal biogenesis factor 7
Cyct	cytochrome c, testis
mEFs	mouse embryonic fibroblasts
PE	phosphatidyl ethanolamine
ePE	ether phosphatidyl ethanolamine
PC	phosphatidyl choline
ePC	ether phosphatidyl choline
U1snRNA	U1 spliceosomal RNA
bs	blind-sterile

References

1. Lazarow PB, Fujiki Y. Biogenesis of peroxisomes. Annu Rev Cell Biol. 1985; 1:489–530. [PubMed: 3916321]
2. Wanders RJ, Waterham HR. Biochemistry of mammalian peroxisomes revisited. Annu Rev Biochem. 2006; 75:295–332. [PubMed: 16756494]
3. Hoepfner D, Schildknegt D, Braakman I, Philippsen P, Tabak HF. Contribution of the endoplasmic reticulum to peroxisome formation. Cell. 2005; 122:85–95. [PubMed: 16009135]
4. Kim PK, Mullen RT, Schumann U, Lippincott-Schwartz J. The origin and maintenance of mammalian peroxisomes involves a de novo PEX16-dependent pathway from the ER. J Cell Biol. 2006; 173:521–532. [PubMed: 16717127]
5. Kunau WH. Peroxisome biogenesis: end of the debate. Curr Biol. 2005; 15:R774–776. [PubMed: 16169481]
6. Purdue PE, Lazarow PB. Peroxisomal biogenesis: multiple pathways of protein import. J Biol Chem. 1994; 269:30065–30068. [PubMed: 7982905]
7. Girzalsky W, Platta HW, Erdmann R. Protein transport across the peroxisomal membrane. Biol Chem. 2009; 390:745–751. [PubMed: 19558328]
8. McNew JA, Goodman JM. An oligomeric protein is imported into peroxisomes in vivo. J Cell Biol. 1994; 127:1245–1257. [PubMed: 7962087]
9. Glover JR, Andrews DW, Rachubinski RA. Saccharomyces cerevisiae peroxisomal thiolase is imported as a dimer. Proc Natl Acad Sci U S A. 1994; 91:10541–10545. [PubMed: 7937990]
10. Gould SJ, Keller GA, Hosken N, Wilkinson J, Subramani S. A conserved tripeptide sorts proteins to peroxisomes. J Cell Biol. 1989; 108:1657–1664. [PubMed: 2654139]
11. Gatto GJ Jr, Geisbrecht BV, Gould SJ, Berg JM. Peroxisomal targeting signal-1 recognition by the TPR domains of human PEX5. Nat Struct Biol. 2000; 7:1091–1095. [PubMed: 11101887]
12. Motley AM, Hettema EH, Hogenhout EM, Brites P, ten Asbroek AL, Wijburg FA, Baas F, Heijmans HS, Tabak HF, Wanders RJ, Distel B. Rhizomelic chondrodysplasia punctata is a peroxisomal protein targeting disease caused by a non-functional PTS2 receptor. Nat Genet. 1997; 15:377–380. [PubMed: 9090382]

13. Braverman N, Steel G, Obie C, Moser A, Moser H, Gould SJ, Valle D. Human PEX7 encodes the peroxisomal PTS2 receptor and is responsible for rhizomelic chondrodysplasia punctata. Nat Genet. 1997; 15:369–376. [PubMed: 9090381]

14. Purdue PE, Zhang JW, Skoneczny M, Lazarow PB. Rhizomelic chondrodysplasia punctata is caused by deficiency of human PEX7, a homologue of the yeast PTS2 receptor. Nat Genet. 1997; 15:381–384. [PubMed: 9090383]

15. Zhang JW, Lazarow PB. PEB1 (PAS7) in Saccharomyces cerevisiae encodes a hydrophilic, intra-peroxisomal protein that is a member of the WD repeat family and is essential for the import of thiolase into peroxisomes. J Cell Biol. 1995; 129:65–80. [PubMed: 7535304]

16. van den Bosch H, Schutgens RB, Wanders RJ, Tager JM. Biochemistry of peroxisomes. Annu Rev Biochem. 1992; 61:157–197. [PubMed: 1353950]

17. Steinberg SJ, Dodt G, Raymond GV, Braverman NE, Moser AB, Moser HW. Peroxisome biogenesis disorders. Biochim Biophys Acta. 2006; 1763:1733–1748. [PubMed: 17055079]

18. Gould SJ, Valle D. Peroxisome biogenesis disorders: genetics and cell biology. Trends Genet. 2000; 16:340–345. [PubMed: 10904262]

19. Shimozawa N. Molecular and clinical aspects of peroxisomal diseases. J Inherit Metab Dis. 2007; 30:193–197. [PubMed: 17347916]

20. Steinberg S, Chen L, Wei L, Moser A, Moser H, Cutting G, Braverman N. The PEX Gene Screen: molecular diagnosis of peroxisome biogenesis disorders in the Zellweger syndrome spectrum. Mol Genet Metab. 2004; 83:252–263. [PubMed: 15542397]

21. White AL, Modaff P, Holland-Morris F, Pauli RM. Natural history of rhizomelic chondrodysplasia punctata. Am J Med Genet A. 2003; 118A:332–342. [PubMed: 12687664]

22. Wanders RJ, Waterham HR. Peroxisomal disorders I: biochemistry and genetics of peroxisome biogenesis disorders. Clin Genet. 2005; 67:107–133. [PubMed: 15679822]

23. Wanders RJ, Dekker C, Hovarth VA, Schutgens RB, Tager JM, Van Laer P, Lecoutere D. Human alkyldihydroxyacetonephosphate synthase deficiency: a new peroxisomal disorder. J Inherit Metab Dis. 1994; 17:315–318. [PubMed: 7807941]

24. Brites P, Waterham HR, Wanders RJ. Functions and biosynthesis of plasmalogens in health and disease. Biochim Biophys Acta. 2004; 1636:219–231. [PubMed: 15164770]

25. Braverman N, Chen L, Lin P, Obie C, Steel G, Douglas P, Chakraborty PK, Clarke JT, Boneh A, Moser A, Moser H, Valle D. Mutation analysis of PEX7 in 60 probands with rhizomelic chondrodysplasia punctata and functional correlations of genotype with phenotype. Hum Mutat. 2002; 20:284–297. [PubMed: 12325024]

26. Brites P, Motley AM, Gressens P, Mooyer PA, Ploegaert I, Everts V, Evrard P, Carmeliet P, Dewerchin M, Schoonjans L, Duran M, Waterham HR, Wanders RJ, Baes M. Impaired neuronal migration and endochondral ossification in Pex7 knockout mice: a model for rhizomelic chondrodysplasia punctata. Hum Mol Genet. 2003; 12:2255–2267. [PubMed: 12915479]

27. Rodemer C, Thai TP, Brugger B, Kaercher T, Werner H, Nave KA, Wieland F, Gorgas K, Just WW. Inactivation of ether lipid biosynthesis causes male infertility, defects in eye development and optic nerve hypoplasia in mice. Hum Mol Genet. 2003; 12:1881–1895. [PubMed: 12874108]

28. Chang B, Hawes NL, Hurd RE, Wang J, Howell D, Davisson MT, Roderick TH, Nusinowitz S, Heckenlively JR. Mouse models of ocular diseases. Vis Neurosci. 2005; 22:587–593. [PubMed: 16332269]

29. Spence SE, Gilbert DJ, Harris BS, Davisson MT, Copeland NG, Jenkins NA. Genetic localization of Hao-1, blind-sterile (bs), and Emv-13 on mouse chromosome 2. Genomics. 1992; 12:403–404. [PubMed: 1310954]

30. Varnum DS. Blind-sterile: a new mutation on chromosome 2 of the house mouse. J Hered. 1983; 74:206–207. [PubMed: 6863898]

31. Hassemer EL, Le Gall SM, Liegel R, McNally M, Chang B, Zeiss CJ, Dubielzig RD, Horiuchi K, Kimura T, Okada Y, Blobel CP, Sidjanin DJ. The waved with open eyelids (woe) locus is a hypomorphic mouse mutation in Adam17. Genetics. 185:245–255. [PubMed: 20194968]

32. Talamas E, Jackson L, Koeberl M, Jackson T, McElwee JL, Hawes NL, Chang B, Jablonski MM, Sidjanin DJ. Early transposable element insertion in intron 9 of the Hsf4 gene results in autosomal recessive cataracts in lop11 and ldis1 mice. Genomics. 2006; 88:44–51. [PubMed: 16595169]

33. Devaiah SP, Roth MR, Baughman E, Li M, Tamura P, Jeannotte R, Welti R, Wang X. Quantitative profiling of polar glycerolipid species from organs of wild-type Arabidopsis and a phospholipase. Dalpha1 knockout mutant Phytochemistry. 2006; 67:1907–1924.
34. Narisawa S, Hecht NB, Goldberg E, Boatright KM, Reed JC, Millan JL. Testis-specific cytochrome c-null mice produce functional sperm but undergo early testicular atrophy. Mol Cell Biol. 2002; 22:5554–5562. [PubMed: 12101247]
35. de Vet EC, Ijlst L, Oostheim W, Wanders RJ, van den Bosch H. Alkyl-dihydroxyacetonephosphate synthase. Fate in peroxisome biogenesis disorders and identification of the point mutation underlying a single enzyme deficiency. J Biol Chem. 1998; 273:10296–10301. [PubMed: 9553082]
36. Carmel I, Tal S, Vig I, Ast G. Comparative analysis detects dependencies among the 5′ splice-site positions. RNA. 2004; 10:828–840. [PubMed: 15100438]
37. Ast G. How did alternative splicing evolve? Nat Rev Genet. 2004; 5:773–782. [PubMed: 15510168]
38. Wang GS, Cooper TA. Splicing in disease: disruption of the splicing code and the decoding machinery. Nat Rev Genet. 2007; 8:749–761. [PubMed: 17726481]
39. Berget SM. Exon recognition in vertebrate splicing. J Biol Chem. 1995; 270:2411–2414. [PubMed: 7852296]
40. Thai TP, Rodemer C, Jauch A, Hunziker A, Moser A, Gorgas K, Just WW. Impaired membrane traffic in defective ether lipid biosynthesis. Hum Mol Genet. 2001; 10:127–136. [PubMed: 11152660]
41. de Vet EC, Ijlst L, Oostheim W, Dekker C, Moser HW, van Den Bosch H, Wanders RJ. Ether lipid biosynthesis: alkyl-dihydroxyacetonephosphate synthase protein deficiency leads to reduced dihydroxyacetonephosphate acyltransferase activities. J Lipid Res. 1999; 40:1998–2003. [PubMed: 10553003]
42. Singh I, Lazo O, Contreras M, Stanley W, Hashimoto T. Rhizomelic chondrodysplasia punctata: biochemical studies of peroxisomes isolated from cultured skin fibroblasts. Arch Biochem Biophys. 1991; 286:277–283. [PubMed: 1680308]
43. Nagan N, Hajra AK, Das AK, Moser HW, Moser A, Lazarow P, Purdue PE, Zoeller RA. A fibroblast cell line defective in alkyl-dihydroxyacetone phosphate synthase: a novel defect in plasmalogen biosynthesis. Proc Natl Acad Sci U S A. 1997; 94:4475–4480. [PubMed: 9114014]
44. Thai TP, Rodemer C, Worsch J, Hunziker A, Gorgas K, Just WW. Synthesis of plasmalogens in eye lens epithelial cells. FEBS Lett. 1999; 456:263–268. [PubMed: 10456321]
45. Komljenovic D, Sandhoff R, Teigler A, Heid H, Just WW, Gorgas K. Disruption of blood-testis barrier dynamics in ether-lipid-deficient mice. Cell Tissue Res. 2009; 337:281–299. [PubMed: 19495798]
46. Teigler A, Komljenovic D, Draguhn A, Gorgas K, Just WW. Defects in myelination, paranode organization and Purkinje cell innervation in the ether lipid-deficient mouse cerebellum. Hum Mol Genet. 2009; 18:1897–1908. [PubMed: 19270340]
47. Bams-Mengerink AM, Majoie CB, Duran M, Wanders RJ, Van Hove J, Scheurer CD, Barth PG, Poll-The BT. MRI of the brain and cervical spinal cord in rhizomelic chondrodysplasia punctata. Neurology. 2006; 66:798–803. discussion 789. [PubMed: 16567694]

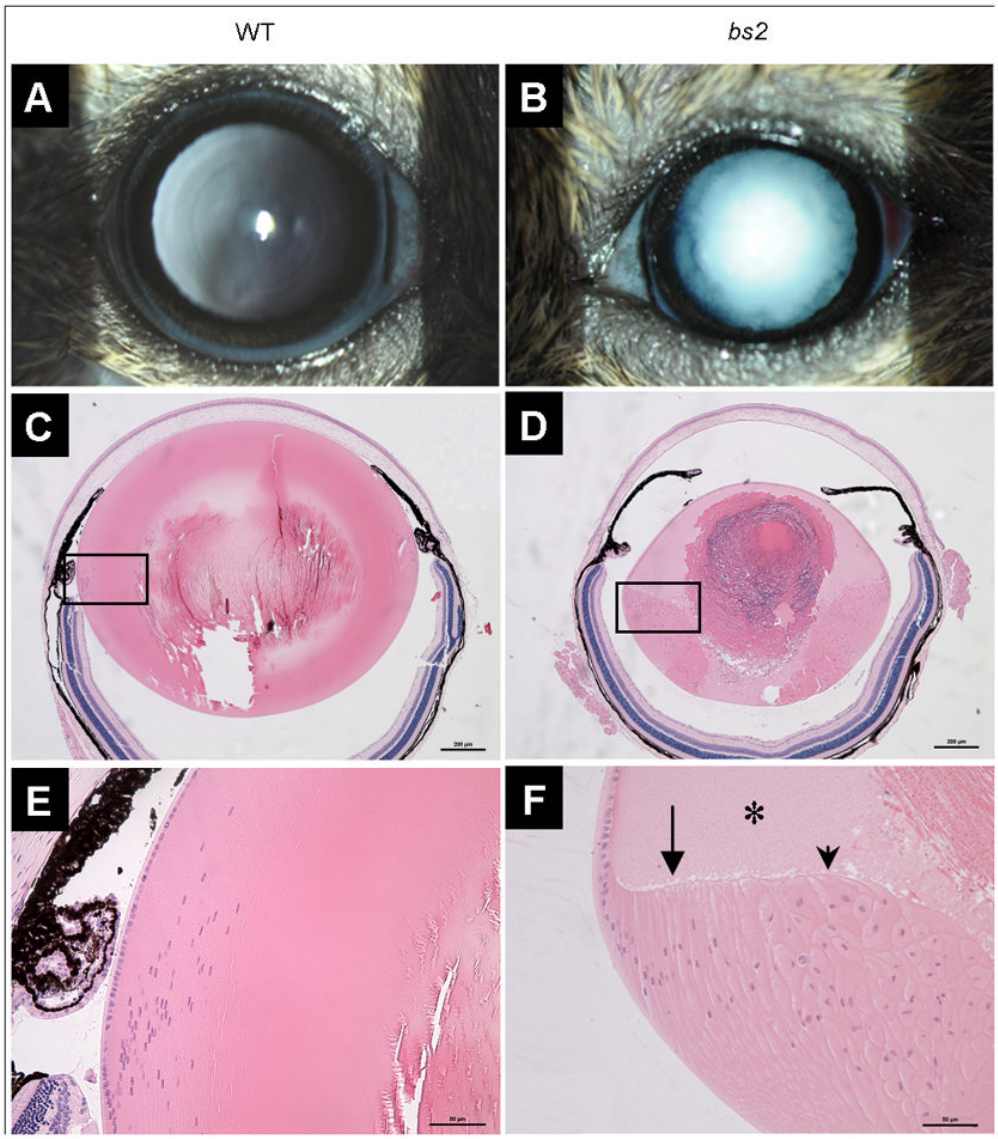

Figure 1.

bs2 eye phenotype. Adult *bs2* mice (B) exhibit nuclear cataracts whereas WT littermate controls have transparent lenses (A). Examination of *bs2* sections, 20x magnification, P28 (D), reveals micropthalmia and a smaller lens as well as a large nuclear cataract compared to the normal WT control (C) (scale bar: 200μm). Boxes indicate regions of 40x magnification in E, F (scale bar: 50μm). *bs2* mice exhibit improper differentiation of lens epithelial cells to fiber cells (F) including vacuolation, morgagnian globules (asterisk), bladder cells (arrowhead), and detachment of the apical-apical junctions of epithelial and fiber cells (arrow).

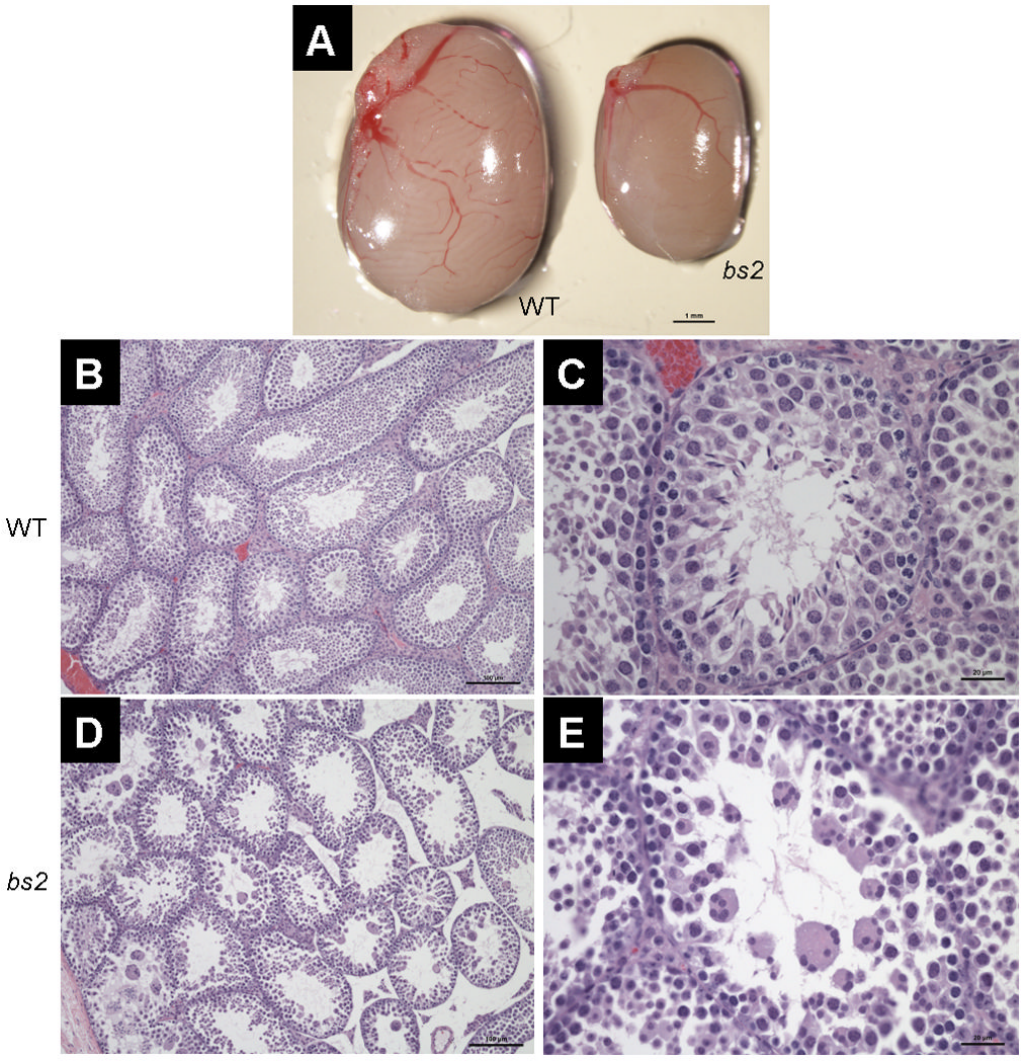

Figure 2.

bs2 testis phenotype. Adult testes from *bs2* mice (A, right) are smaller than WT siblings (A, left, scale bar: 1mm). Histological analysis of adult testis reveals that in *bs2* mice (D, 10x) the seminiferous tubules are severely disrupted (scale bar: 100μm). Higher magnification (C, E, 40x) reveals that bs2 tubules contain no mature spermatozoa but do contain large multinucleate cells (scale bar: 20μm)

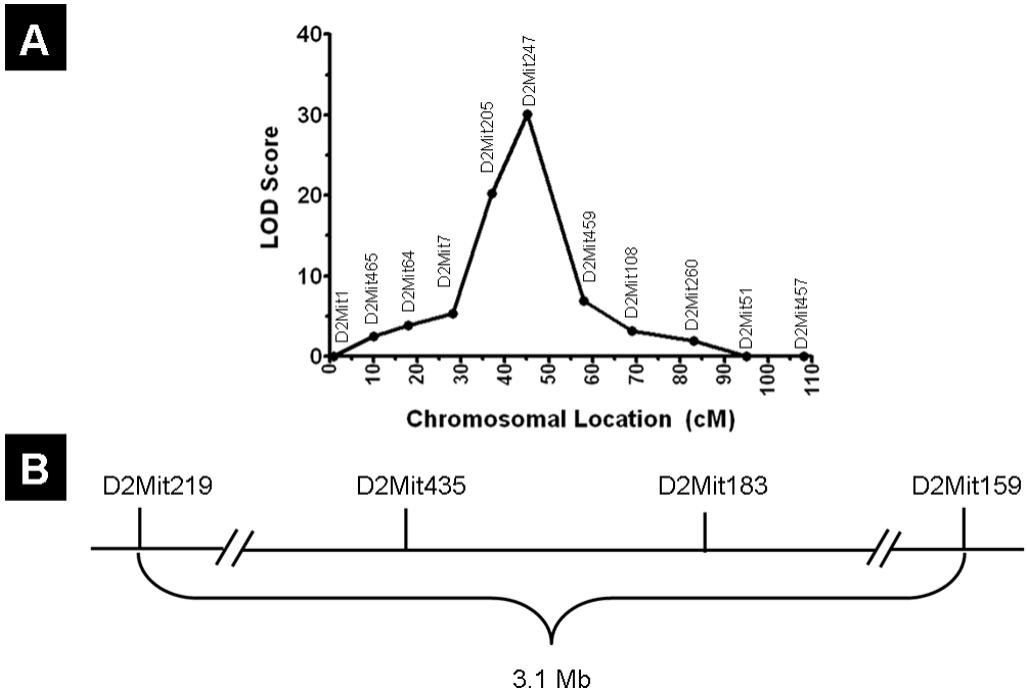

Figure 3.

Linkage mapping and mutation identification. (A) Microsatellite markers were used to identify linkage to mouse chromosome 2, approximately 45 cM distal from the centromere. (B) Fine mapping narrowed the critical region to 3.1 Mb, between *D2Mit219* and *D2Mit159*.

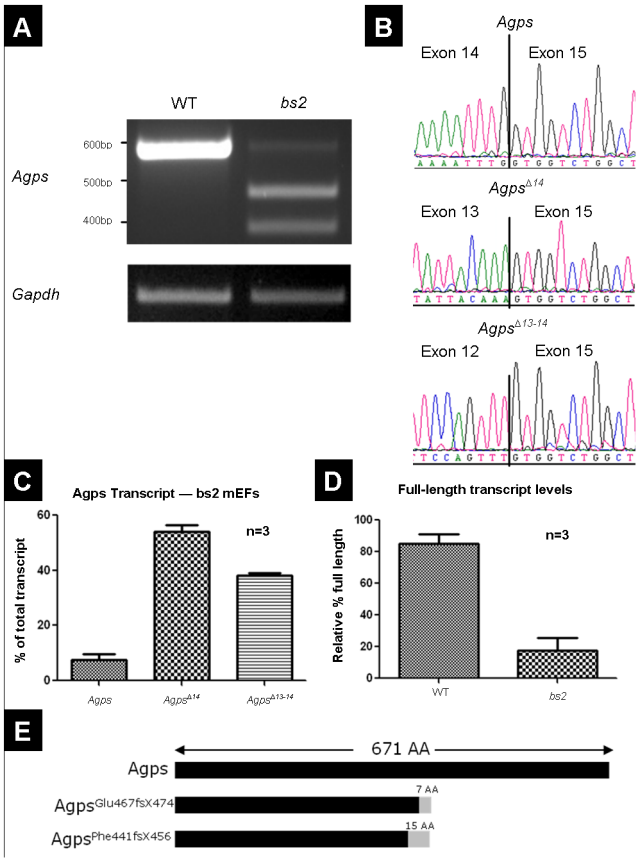

Figure 4.

Alternative splicing of *Agps* transcript in *bs2* mice. (A) RT-PCR from mEF cDNA amplified three products in *bs2* mice: 564bp, 451bp, and 371bp. In contrast, only the WT 564bp band was observed in WT controls. (B) Sequencing of the DNA contained in these bands identified the 564bp band as the full-length transcript, the 451bp band as skipping exon 14 (*Agps* $^{\Delta 14}$), and the 371bp band as skipping exons 13 and 14 (*Agps* $^{\Delta 13–14}$). (C) Semi-quantitative RT-PCR shows that 7% of *Agps* transcript was full-length, 55% *Agps* $^{\Delta 14}$, and 38% *Agps* $^{\Delta 13–14}$. (D) Semi-quantitative PCR also reveals that full length *Agps* transcript was present at 15% the level of that seen in WT controls. ($p<0.05$ for C, D) (E) Agps^{Glu467fsX474} and Agps^{Phe441fsX456}, putative proteins formed from *Agps* $^{\Delta 14}$ and *Agps* $^{\Delta 13–14}$ transcripts, would contain an immediate frameshift at the beginning of exon 15, followed by 7 or 15 amino acids of nonsense, as well as a premature stop codon.

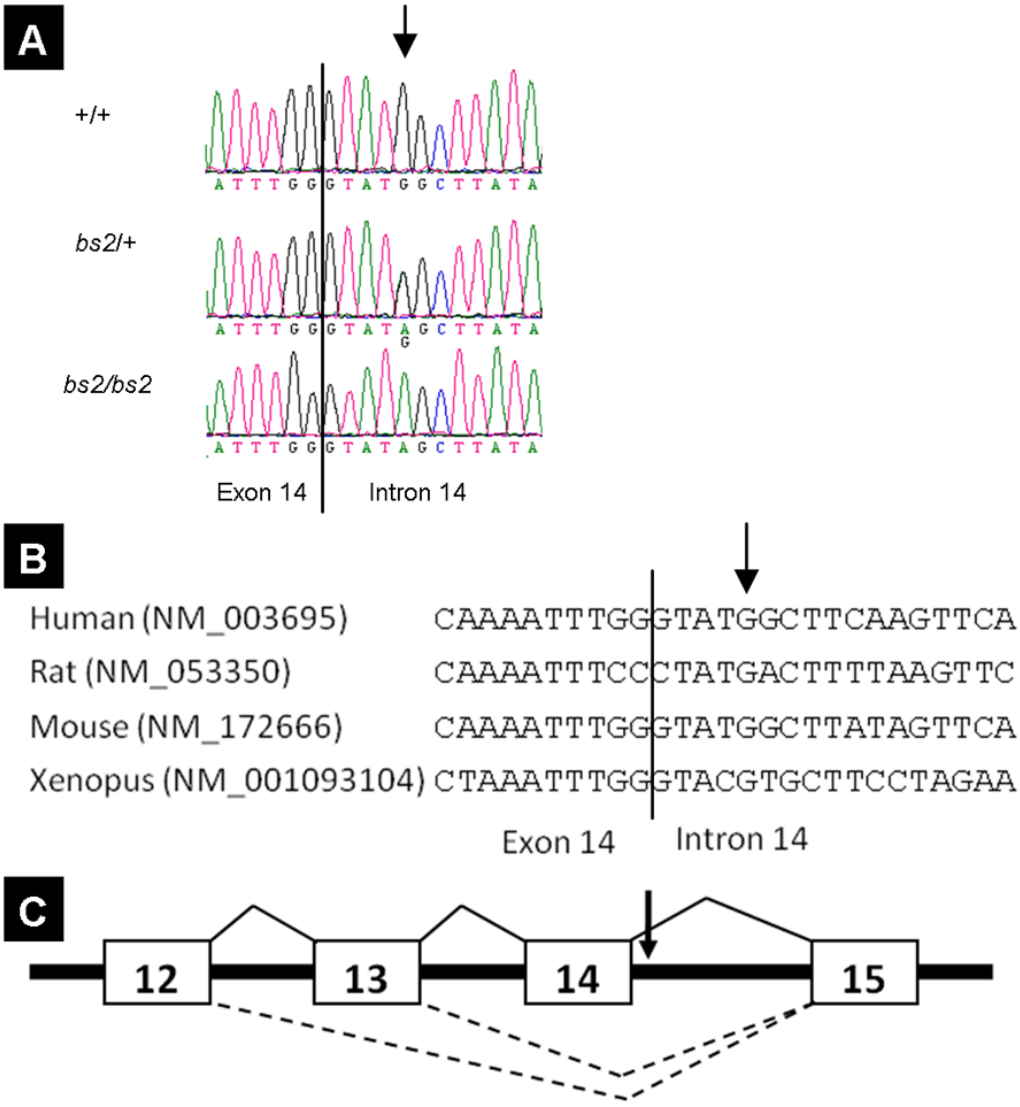

Figure 5.

Identification of a single-base pair substitution in *Agps* intron 14. (A) A single base pair substitution, IVS14+5G>A, was identified in *bs2* mice. All affected F2 mice genotyped A/A while unaffected mice genotyped G/A or G/G. (B) IVS14+5G is a key nucleotide within the 5′ splice donor site, which is conserved in human, rat, mouse, and xenopus. (C) IVS14+5 G>A disrupts a conserved splice-donor sequence (arrow). In the absence of this nucleotide, splice donor sites from intron 12 or 13 compete for the intron 14 splice acceptor, resulting in the *Agps* $^{\Delta 13–14}$ and *Agps* $^{\Delta 14}$ products.

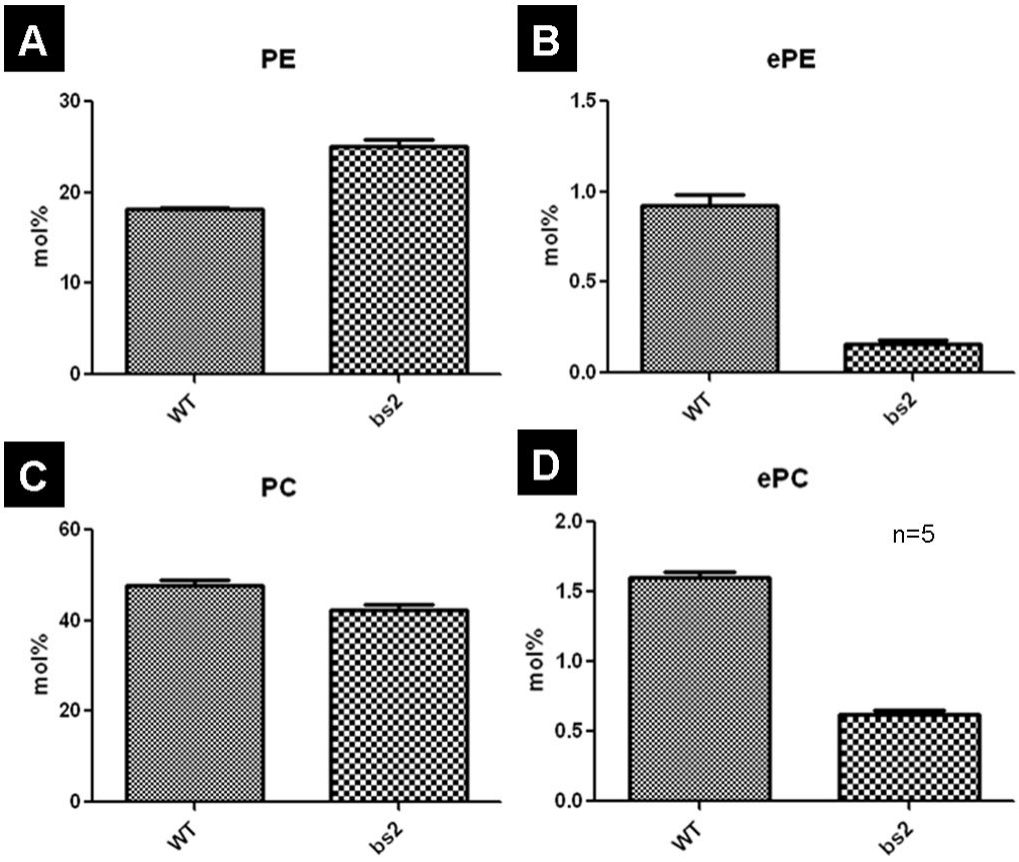

Figure 6.

Mass spectrometry analysis of lipid species from brain lipid extracts. Ether-phosphatidylethanolamine (ePE; B) and ether phosphatidylcholine (ePC; D) were both significantly lower in *bs2* mice ($p<0.0001$, both). Phosphatidylcholine (PC; C) levels are also lower in *bs2* mice ($p=0.0089$), while phosphatidylethanolamine (PE; A) levels are higher ($p<0.0001$) in *bs2* brains. Five replicates were performed for each genotype and significance was calculated via a t-test.

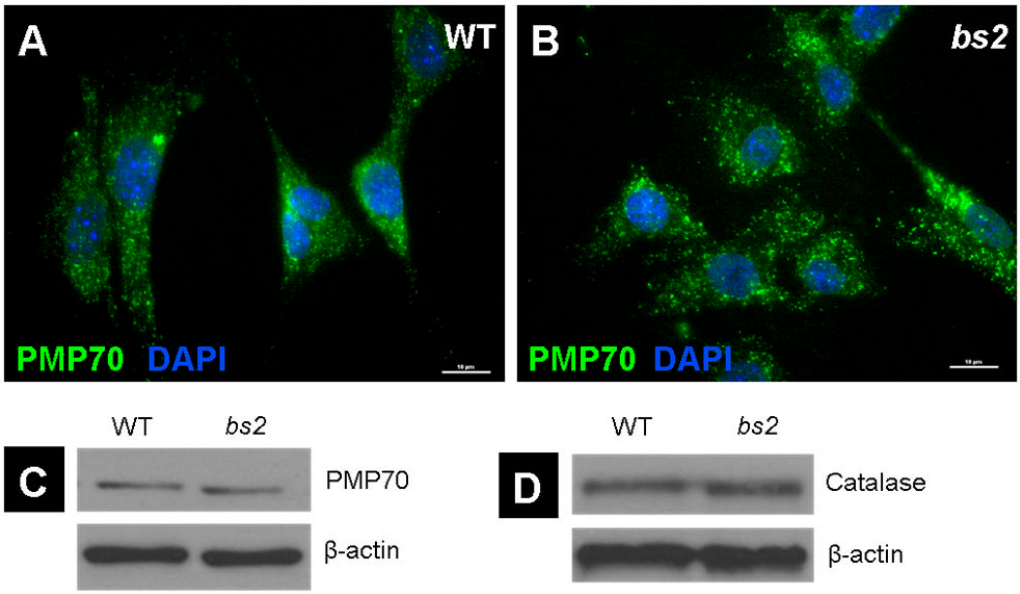

Figure 7.

Peroxisomal assembly and PTS-mediated protein import. Immunofluorescent staining of Peroxisomal membrane protein 70 (PMP70, Green) counterstained with DAPI (Blue) confirms the presence of peroxisomes in *bs2* mEFs (B) with no noted morphological deviations from those seen in WT controls (A) (scale bars: 10μm). Protein levels of PMP70 (C) and catalase (D) were not significantly different between WT and *bs2* samples, as evaluated by western blot.